Title

Brain microstructural correlates of visuospatial choice reaction time in children

Journal

NeuroImage, 58(4)

ISSN

1053-8119

Authors

Madsen, Kathrine Skak
Baaré, William FC
Skimminge, Arnold
et al.

Publication Date

2011-10-01

DOI

10.1016/j.neuroimage.2011.07.032

Peer reviewed

NeuroImage 58 (2011) 1090–1100

Contents lists available at ScienceDirect

NeuroImage

journal homepage: www.elsevier.com/locate/ynimg

Brain microstructural correlates of visuospatial choice reaction time in children

Kathrine Skak Madsen [a,b,c,*], William F.C. Baaré [a,b], Arnold Skimminge [a], Martin Vestergaard [a], Hartwig R. Siebner [a,b,c], Terry L. Jernigan [a,b,c,d]

[a] Danish Research Centre for Magnetic Resonance, Copenhagen University Hospital, Hvidovre, Denmark
[b] Center for Integrated Molecular Brain Imaging, Copenhagen, Denmark
[c] Faculty of Health Sciences, University of Copenhagen, Copenhagen, Denmark
[d] Center for Human Development, University of California, San Diego, La Jolla, CA, USA

ARTICLE INFO

Article history:
Received 26 April 2011
Revised 26 June 2011
Accepted 9 July 2011
Available online 21 July 2011

Keywords:
Brain maturation
Grey matter microstructure
Diffusion tensor imaging
Motor function development
Reaction time
Striatum

ABSTRACT

The corticospinal tracts and the basal ganglia continue to develop during childhood and adolescence, and indices of their maturation can be obtained using diffusion-weighted imaging. Here we show that a simple measure of visuomotor function is correlated with diffusion parameters in the corticospinal tracts and neostriatum. In a cohort of 75 typically-developing children aged 7 to 13 years, mean 5-choice reaction times (RTs) were assessed. We hypothesised that children with faster choice RTs would show lower mean diffusivity (MD) in the corticospinal tracts and neostriatum and higher fractional anisotropy (FA) in the corticospinal tracts, after controlling for age, gender, and handedness. Mean MD and/or FA were extracted from the right and left corticospinal tracts, putamen, and caudate nuclei. As predicted, faster 5-choice RTs were associated with lower MD in the corticospinal tracts, putamen, and caudate. MD effects on RT were bilateral in the corticospinal tracts and putamen, whilst right caudate MD was more strongly related to performance than was left caudate MD. Our results suggest a link between motor performance variability in children and diffusivity in the motor system, which may be related to: individual differences in the phase of fibre tract and neostriatal maturation in children of similar age, individual differences in motor experience during childhood (i.e., use-dependent plasticity), and/or more stable individual differences in the architecture of the motor system.

Introduction

Perceptual–motor speed continues to develop throughout childhood and adolescence (Kail, 1991), yet little is known about how increasing perceptual–motor expertise is related to structural brain development. Increasing speed of processing can involve a wide range of sensory, cognitive and motor functions, and has been studied at the behavioural level with many different choice reaction time (RT) tasks (Konrad et al., 2009; Madden et al., 2004; Miller and Low, 2001). In this study, we wished to clarify whether choice RT on a simple behavioural task was correlated with microstructure within the motor network. Facilitation and execution of voluntary movements are mediated by a cortical-striatal-pallidal-thalamic-motor cortical network, also referred to as the *direct* pathway. Activation of the *direct* pathway is mediated by cortical inputs from the motor cortices to the neostriatum, which sends inhibitory signals to the internal segment of globus pallidus. This reduces the inhibitory tone on the thalamus, which results in thalamic activation of cortical regions (Haber and Gdowski, 2004), allowing activation of selected motor responses via the major output pathway, the corticospinal tract (CST). In the present study, our focus was on core motor brain structures, namely the CST, and the neostriatum (putamen and caudate nuclei), which have been implicated in movement selection, initiation and execution (Bohr et al., 2007; Gerardin et al., 2004; Haber and Gdowski, 2004).

The CSTs and neostriatum continue to develop during childhood and adolescence (Jernigan et al., 1991; Lebel et al., 2008; Sowell et al., 1999), and indices of their maturation can be obtained using diffusion-weighted imaging (DWI). DWI is sensitive to the diffusion of water molecules. In white matter, water diffusion is less hindered parallel than perpendicular to the fibre bundles, ostensibly due to occluding cellular structures, i.e., axonal membranes and surrounding myelin sheaths, causing diffusion anisotropy. In subcortical grey matter, water diffusion is also hindered by occluding cell membranes (neuronal and glial), but since the membranes are not highly parallel, the diffusion is relatively isotropic (at clinical voxel sizes) (Beaulieu, 2009). By employing the diffusion tensor model, useful measures can be derived, including fractional anisotropy (FA) estimating the degree of diffusion directionality, mean diffusivity (MD), and diffusivity parallel ($\lambda_{||}$) and perpendicular ($\lambda\perp$) to the principal diffusion direction (Basser et al., 1994; Beaulieu, 2009).

* Corresponding author at: Danish Research Centre for Magnetic Resonance, Copenhagen University Hospital, Hvidovre, Kettegaard Allé 30, DK-2650 Hvidovre, Denmark. Fax: +45 36470302.
E-mail address: Kathrine@drcmr.dk (K.S. Madsen).

1053-8119/$ – see front matter © 2011 Elsevier Inc. All rights reserved.
doi:10.1016/j.neuroimage.2011.07.032

Studies applying DWI in children and adolescents have reported age-related increases in FA and/or decreases in MD in multiple locations within white matter, possibly due to ongoing myelination and/or an increase in axonal diameter or density (Eluvathingal et al., 2007; Lebel et al., 2008; Snook et al., 2005). Further, age-related increases in FA and decreases in MD have also been reported in several subcortical grey matter structures (Lebel et al., 2008; Snook et al., 2005), but the underlying neural changes causing this are largely unknown. Lebel et al. (2008) observed that diffusion parameters within the motor network, including the CST, putamen, and caudate nuclei, exhibit protracted age-related changes continuing into early adulthood. Focusing on the subjects studied by Lebel et al. (2008) within the current sample's age range (7 to 13 years), strong age-related reductions in MD are apparent in both CSTs and neostriatal structures across this range. Age-related increases in FA were also prominent in CSTs, but neostriatal FA changes were more variable, and less strongly related to age, in this age group.

A growing number of DWI studies in children have linked regional white matter microstructure to performance levels on, e.g., reading (Niogi and McCandliss, 2006), response inhibition (Madsen et al., 2010), and working memory (Vestergaard et al., 2011) tasks. In healthy young right-handed adults, faster right- relative to left-handed responses have been correlated with higher FA in the left corticospinal tract in an auditory simple reaction time task (Bohr et al., 2007). However, no studies have examined the relationship between the microstructure of motor pathways and perceptual–motor speed as reflected by choice RT in developing children. Here we tested the hypotheses that in typically-developing children faster 5-choice RT would be associated with lower MD in the CSTs and neostriatum, and higher FA in the CSTs, independently of age. That is that even in children of similar age, those with a more mature pattern of lower MD and higher FA within the motor network would exhibit better RT performance, than those with a less mature pattern.

Materials and methods

Subjects

Ninety-two typically-developing children and adolescents (53 girls, 39 boys) aged 7 to 13 years from three schools (1st–6th graders) in the Copenhagen suburban area participated in the study. Prior to participation and after receiving oral and written explanation of the study aims and study procedures, all children assented to the procedures and informed written consent was obtained from the parents/guardians of all subjects. According to parent reports, no subjects had any known history of neurological or psychiatric disorders or significant brain injury. The study was approved by the local Danish Committee for Biomedical Research Ethics (H-KF-01-131/03) and conducted in accordance with the Declaration of Helsinki.

Seventeen (10 girls, 7 boys) of the 92 recruited children were subsequently excluded from further analyses because of technical problems with the behavioural task (1 subject), incidental findings on MRI (1 subject), reduced DWI image quality as described below (12 subjects) or because they did not complete the scanning session (3 subjects). There were no significant differences between the 75 included and the 17 excluded subjects with respect to age, gender, parental education, or handedness (as assessed with the Edinburgh handedness inventory). Demographic data from the 75 included subjects are presented in Table 1.

Table 1
Demographic data for the 75 included subjects[a].

	1st/2nd graders	3rd/4th graders	5th/6th graders	All
Age (mean ± std)	8.26 ± 0.46	10.11 ± 0.37	12.1 ± 0.42	10.17 ± 1.59
Gender (female/male)	13/10	16/13	14/9	43/32
Handedness (right/left)	20/3	25/4	21/2	66/9
Parents' average years of education (mean ± std)	14.0 ± 1.7	13.4 ± 2.0	13.7 ± 2.0	13.7 ± 1.9

[a] Children enrolled in the study were scanned either in the months just before (when in 1st, 3rd or 5th grade) or just after (when in 2nd, 4th or 6th grade) the summer holiday.

Reaction time task

The experimental task consisted of a computerised visuospatial 5-choice RT task implemented in the Cambridge Neuropsychological Test Automated Battery (Cambridge Cognition Ltd., Cambridge, UK), and was the first test out of a series of tests within a 1.5 hour test battery. The task required detection of a spatially-varying visual target stimulus and selection, initiation, and execution of a manual response spatially matched to that target. The children were sitting in front of a touch screen and were instructed to press a button on a response pad with the index finger of the dominant hand. After a random delay, between 750 and 2250 ms, a yellow dot was presented in one of the circles displayed on the screen, and subjects were required to release the button and touch the yellow dot on the screen as fast as possible. In an initial block of trials, the yellow dot appeared in a single circle located centrally on the screen. In the subsequent block of 5-choice trials, the yellow dot appeared (randomly) in one of five circles visible on the screen (Fig. 1). Both blocks were divided into a practice and a test phase. The training phases each consisted of 5 trials. Subjects who failed to perform 4 of the 5 practice trials correctly received a second practice phase before the test phase. Each test phase consisted of 15 trials.

For each block, button release time, movement time, and accuracy scores were recorded. The behavioural measure used to test the hypotheses was button release time for the 5-choice test trials (referred to as 5-choice RT), which estimates the time taken to select and initiate the movement. Error rates were very low (47 of 75 subjects produced no errors). However, data from error trials were excluded from the calculations. Z-scores for trial RTs were computed within each subject (by block) and trials with a Z-score above 3 were excluded (as outliers) from the calculation of the mean RTs.

Movement times were not used for the analyses, because this measure clearly reflected not only individual differences in movement speed, but also individual differences in response style. The subjects were required to physically touch the display screen. Some subjects consistently decelerated their movements as they approached the screen in order to touch it softly, whilst others elected to stab the screen with more force.

Image acquisition

All subjects were scanned using a 3T Siemens Magnetom Trio MR scanner (Siemens, Erlangen, Germany) with an eight-channel head coil (Invivo, FL, USA). All acquired scans were aligned parallel to the anterior commissure–posterior commissure line. T_1-weighted images of the whole head were acquired using a 3D MPRAGE sequence (TR = 1550 ms, TE = 3.04 ms, matrix 256 × 256, 192 sagittal slices, 1 × 1 × 1 mm^3 voxels, acquisition time = 6:38). T_2-weighted images of the whole head were acquired using a 3D turbo spin echo sequence (TR = 3000 ms, TE = 354 ms, FOV = 282 × 216, matrix = 256 × 196, 192 sagittal slices, 1.1 × 1.1 × 1.1 mm^3 voxels, acquisition time = 8:29). Whole brain diffusion-weighted (DW) images were acquired using a twice-refocused balanced spin echo sequence that minimised eddy current distortion (Reese et al., 2003). Ten non-DW images (b = 0) and 61 DW images (b = 1200 s/mm^2), encoded along independent collinear diffusion gradient orientations, were acquired (TR = 8200 ms, TE = 100 ms, FOV = 220 × 220, matrix = 96 × 96, GRAPPA: factor = 2, 48 lines, 61 transverse slices with no gap, 2.3 × 2.3 × 2.3 mm^3 voxels,

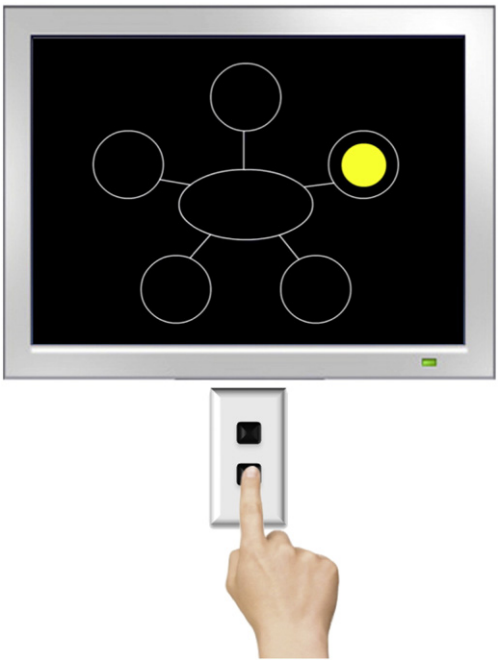

Fig. 1. Set-up of the 5-choice reaction time (RT) task. Subjects sit in front of a touch screen and are instructed to press a button on a pad in front of them. After a random delay, a yellow dot appears in one of five circles. Subjects must release the button as quickly as possible and touch the yellow dot. The 5-choice RT was defined as the average time it took to release the button on accurate choice RT trials.

acquisition time = 9:50). A gradient echo field map was acquired to correct B_0 field distortions (TR = 530 ms, TE[1] = 5.19 ms and TE[2] = 7.65 ms, FOV = 256 × 256; matrix = 128 × 128, 47 transverse slices with no gap, voxel size = 2 × 2 × 3 mm^3, acquisition time = 2:18).

Image evaluation

All subjects' images were evaluated by an experienced neuroradiologist. Prior to image analysis, and blind to behavioural data, the raw images from all subjects were visually inspected to ascertain the quality of the data. Based on this inspection, 12 subjects were deemed to have significantly reduced DW image quality due to movement or susceptibility artefacts and were excluded from further analysis. An additional 6 subjects (*3 boys and 3 girls*, *3 right- and 3 left-handers*) had reduced T_1-weighted image quality and were not included in analyses involving grey matter regions-of-interest (ROIs), but were included in all other analyses.

Image preprocessing

Images were preprocessed using pipelines implemented in Matlab, using mainly SPM5 (Wellcome Department of Cognitive Neurology, University College London, UK) routines. T_1-weighted and T_2-weighted images were corrected for spatial distortions due to non-linearity in the gradient system of the scanner (Jovicich et al., 2006). The T_2-image was coregistered (no reslicing), using a 6-parameter mutual information rigid transformation to the T_1-image. In the DWI analysis, each subject's mean b0 image was coregistered (no reslicing), to the T_2-image, after which all DW images were coregistered (no reslicing) to the mean b0 image. Next, all coregistered images were corrected for geometric distortions using a voxel displacement map based on both the acquired B_0 field map (Andersson et al., 2001) and the scanner specific gradient non-linearities (Jovicich et al., 2006). Finally, all images were resliced using trilinear interpolation. Note that this procedure involves only one reslicing step. The diffusion gradient orientations were adjusted to account for any rotation applied during registration. The diffusion tensor was fitted using the RESTORE algorithm with a noise standard deviation of 30 (Chang et al., 2005) implemented in Camino, and fractional anisotropy (FA), mean diffusivity ($MD = (\lambda_1 + \lambda_2 + \lambda_3)/3$) as well as diffusivity parallel ($\lambda_{||} = \lambda_1$) and perpendicular ($\lambda\perp = (\lambda_2 + \lambda_3)/2$) to the principal diffusion direction were calculated. A brain mask based on the T_2-weighted image was applied to the FA and diffusivity images.

Inter-subject spatial normalisation of fibre tracts

In the present study, we extracted FA and diffusivity measures from regions-of-interest (ROIs) to test specific hypotheses and to determine the anatomical specificity of observed associations (see below). Spatial normalisation and alignment of fibre tracts across subjects were achieved using the Tract-Based Spatial Statistics (TBSS) module (Smith et al., 2006), part of FSL 4.1.4 (Smith et al., 2004). At first, all subjects' FA images were aligned into a common space using the non-linear registration tool FNIRT (Andersson et al., 2007). A study-specific target, the group's most representative FA image, was then identified after non-linearly registering each subject's FA image to every other subject's FA image. Next, the target FA image was aligned to MNI space using affine registration and subsequently the entire aligned dataset was transformed into 1 mm^3 MNI space. A cross-subject mean FA image was created and thinned to create a mean FA skeleton, representing the centres of all tracts common to the group. The mean FA skeleton was thresholded at FA>0.25, and contained 103,588 1 mm^3 interpolated isotropic voxels, corresponding to approximately one quarter of the voxels with FA above 0.25. Each subject's aligned FA image was then projected onto the mean skeleton by locating the highest local FA value in the direction perpendicular to the skeleton tracts and assigning this value to the skeleton. Finally, a symmetric mean FA map based on the average of the mean FA map and its left-right flipped counterpart was generated, and subsequently thinned and masked with a (one voxel) dilated version of the original skeleton in order to generate a symmetric mean skeleton. The symmetric mean skeleton contained 102,154 voxels. In addition, the nonlinear warps, skeleton projections and symmetric skeleton generation were applied to the MD, $\lambda_{||}$ and $\lambda\perp$ data.

Inter-subject spatial normalisation of grey matter

Both T_1 and T_2 images were processed using the VBM5 toolbox in SPM5 (http://dbm.neuro.uni-jena.de/vbm/vbm5-for-spm5/), which includes a unified segmentation algorithm (Ashburner and Friston, 2005) and a Hidden Markov Random Field (HMRF) method (Cuadra et al., 2005). T_2-weighted images were used to create brain masks in native space. Resulting brain masked grey and white matter tissue maps in native space, the affine part of the spatial transformation from native to MNI space (obtained from the VBM5 analysis), and their left-right flipped counter parts were subsequently used in DARTEL ("Diffeomorphic Anatomical Registration Through Exponentiated Lie Algebra") using default settings (Ashburner, 2007), for high-dimensional inter-subject registration. Including the left-right flipped tissue maps ensured that resulting flow fields that parameterize the deformations were symmetric. Using the final symmetric flow fields, the native T_1-images were warped into average symmetric image space ('DARTEL space').

Regions-of interest (ROIs)

White matter ROIs

ROIs were drawn onto the mean symmetric skeleton overlaid on the mean symmetric FA image using FSLview. Corticospinal tract (CST) ROIs (Figs. 2a,c) were delineated using information from the probabilistic fibre atlas (Hua et al., 2008) implemented in FSLview.

The CST ROIs included skeleton segments extending from the motor cortex (hand area) and the sensorimotor cortex, and down through the posterior limb of the internal capsule. No skeleton voxels inferior to slice Z = −20 were included in the ROIs. Further, the ROIs were located between slice Y = −10 to −35. The ROIs each contained 2434 voxels. Mean FA, MD, $\lambda_{||}$ and $\lambda\perp$ values from the left and right CST, and from the whole skeleton were extracted for each subject (N = 75) for statistical analyses. Note that for the left-handed subjects, the left and right CST ROI values were flipped after extraction, so that data corresponded with the contra- and ipsilateral CST to the dominant hand, which was used in the RT task, i.e. left CST for the right-handed subjects and right CST for the left-handed subjects corresponds to the contralateral CST.

Grey matter ROIs

ROIs of the caudate nuclei and putamen were constructed to extract the MD, FA $\lambda_{||}$, $\lambda\perp$, and volume of these structures from each subject (N = 69). Striatal cell bridges were not included in any of the ROIs. The posterior border of the caudate nucleus ROI was the most posterior coronal slice where the putamen was visible, and thus the posterior part of the tail of the caudate nucleus was excluded. In order to examine the anatomical specificity of the neostriatal effects, we constructed an ROI of nearby, but functionally distinct, subcortical grey matter, namely the combined nucleus accumbens (nAcc) and amygdala (nAcc/amygdala). This ROI thus serves as a control region for comparison to the neostriatal ROIs. ROIs were drawn onto the symmetric average of the DARTEL-warped T_1-images of all subjects (Figs. 2b,c).

To ensure that the striatal ROIs for which MD was extracted included only fully-volumed grey matter, an approximately one-voxel thick layer of grey matter at the outer border was not included. Resulting binary ROIs were resliced into native T_1-space using inverse deformation fields and trilinear interpolation, and then binarized using a threshold of 0.5. Next, ROIs were overlaid on native T_1-images to visually inspect the anatomical fit of the ROIs for each individual subject. To transform ROIs from native T_1-space to native DTI space all subjects' FA images were warped to the subject's own native T_1-image using FNIRT. Using the inverse warp field, ROIs were resliced into native DTI space using trilinear interpolation and binarized. Again, the anatomical fit of the ROIs was visually inspected (Fig. 2b). The binary ROIs were multiplied with the subjects' own FA image thresholded at FA<0.25 to exclude potential white matter (partially-volumed) voxels. The mean (±standard deviation (std)) volume of the ROIs, from which MD were extracted, were: left putamen = 4311 (±432), right putamen = 4011 (±444), left caudate nucleus = 2750 (±348), right caudate nucleus = 2918 (±372), left nAcc/amygdala = 1093 (±120), and right nAcc/amygdala = 1093 (±120). Mean MD and FA values were extracted from all ROIs for each subject and used in statistical analyses.

Four ROIs including the *whole* left and right putamen and caudate nuclei were delineated to estimate the volumes of these structures. The mean (±std) number of 1 mm^3 voxels in the ROIs were: left putamen = 4544 (±460), right putamen = 4562 (±455), left caudate nucleus = 3954 (±424), right caudate nucleus = 3954 (±443). Further, total brain volume was extracted from all subjects (mean ± std = 1300, 289 ± 118,353). For use in statistical analyses, relative volumes of the putamen and caudate were calculated: (ROI/brain volume).

Note that for the left-handed subjects, the values of the left and right ROIs were flipped after extraction, to yield ROIs that were contra- and ipsilateral to the dominant hand.

Statistical analysis

Statistical analyses were performed in SPSS software (SPSS 19, SPSS Inc., Chicago, USA). Analyses involving white matter ROIs were based on 75 individuals, whilst analyses involving grey matter ROIs included data from 69 individuals. Two-tailed t-tests were used to compare boys and girls on the behavioural and ROI measures. Age effects on the behavioural and ROI measures, adjusted for gender and handedness, were examined using linear regression models.

Specific hypotheses were tested using multiple linear regression models. To fulfil assumptions of normality of the residuals, mean RTs were transformed using the equation: 1 − (1/mean RT). After transforming the behavioural data, all data were approximately normally distributed according to Shapiro–Wilk tests. All other assumptions for linear regression were fulfilled. The statistical tests were performed hierarchically.

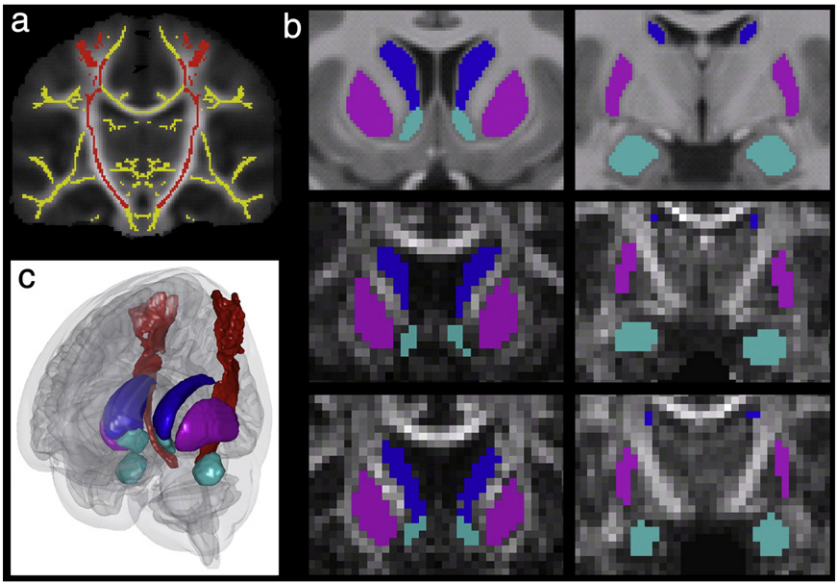

Fig. 2. (a) The corticospinal tract ROIs in red and the symmetric TBSS skeleton in yellow overlaid on the group mean symmetric FA map. (b) In the top images, 'DARTEL' space ROIs in the putamen (magenta), caudate nucleus (blue), and the combined nucleus accumbens and amygdala (cyan) overlaid on the symmetric average of the DARTEL-warped T_1-images of all subjects. The four images in the bottom right illustrate the thresholded ROIs in native DWI space of two individuals. (c) Smoothed 3D versions of the ROIs depicted together with a representation of the right hemisphere of the symmetric average DARTEL-warped grey and white matter segmentations.

Our main hypotheses were that faster 5-choice RT would be associated with lower MD in the CSTs and neostriatum as well as with higher FA in the CSTs, after adjusting for age, gender and handedness. These hypotheses were tested at a statistical threshold of $p \leq 0.017$ (Bonferroni corrected for 3 tests), whilst follow-up analyses were considered significant when $p \leq 0.05$.

Planned follow-up analyses were contingent on observing significant associations with MD or FA in the primary analyses. Follow-up analyses were performed 1) to assess the anatomical specificity of the effects, either by adjusting for whole skeleton MD in models with CST MD, or by adjusting for nAcc/amygdala MD in models with neostriatal MD; 2) to assess the contribution of the ipsi- and contralateral ROIs to the effects; and 3) to determine whether a measure of simple RT mediated the effects on choice RT. To further explore the nature of the observed CST MD effects, $\lambda_{||}$ and $\lambda\perp$ were examined, since these diffusion parameters sometimes provide additional information about the underlying white matter microstructure. Additional planned follow-up analyses were performed to assess the relative contributions of putamen and caudate nucleus MD, as well as the degree to which putamen and caudate volumes may have contributed to the observed effects. To further explore the nature of the observed neostriatal effects, post hoc analyses assessed the relationship between 5-choice RT and caudate and putamen FA, $\lambda_{||}$ and $\lambda\perp$.

Finally, based on the results, post hoc analyses were performed on caudate MD to assess whether the effect was lateralized, by modelling ipsi- and contralateral caudate MD simultaneously, at first for the whole subject group, and then for the right- and left-handers separately.

Two effect-size maps are presented to provide further anatomical information about the association between MD and 5-choice RT across the white matter skeleton and the neostriatum (Jernigan et al., 2003). Both maps were based on the right-handed subjects only, and included data from, respectively, 66 and 63 subjects for the skeleton map and the neostriatum map. The effect-size maps are t-maps of the correlation between MD and 5-choice RT, adjusted for age and gender. Positive correlations, i.e., lower MD with faster 5-choice RTs, are shown in warm colours (red to yellow). The effect-size map of the neostriatum was based on the warped MD image smoothed with a 4 mm FWHM Gaussian kernel.

Results

Simple and 5-choice RTs and diffusion parameter measures of the ROIs are summarised in Table 2. Separate statistics are provided for boys and girls, but none of the gender differences on RT or the diffusion measures approached significance (ps>0.17), except for putamen MD ($p = 0.043$) and nAcc/amygdala MD ($p = 0.055$). Scatterplots of the relationship between age and the main variables are shown in Fig. 3. Significant age effects, after adjusting for gender and handedness, were observed on the behavioural measures (*5-choice RT*: $p = 10^{-7}$; *simple RT*: $p = 10^{-6}$) and on the ROI MD measures (*CST*: $p = 0.00004$; *neostriatal*: $p = 0.00008$; *nAcc/amygdala*: $p = 0.05$) and motor ROI FA measures (*CST*: $p = 0.0004$; *neostriatal*: $p = 0.002$) measures, but not on nAcc/amygdala FA ($p = 0.33$) or the neostriatal volumes ($ps \geq 0.15$). All models below were adjusted for age, gender and handedness, unless otherwise noted.

Associations between 5-choice RT and diffusion parameters of the corticospinal tract

Results obtained from the regression models that tested our main hypotheses regarding diffusion parameters of the CST are listed in Table 3, where each row represents a separate planned model predicting 5-choice RT. As hypothesised, faster 5-choice RT was significantly associated with lower CST MD (Table $3_{(2)}$, Fig. 4a). The association became stronger when excluding age from the model (Table $3_{(2a)}$). No significant association was found between 5-choice RT and CST FA (Table $3_{(1)}$).

Table 2
Mean ± standard deviation of the behavioural measures and DTI measures within the regions-of-interest.

	All subjects	Girls	Boys
Behavioural measure			
Mean 5-choice RT (ms)[a]	357.3 ± 59.9	361.2 ± 65.8	352.0 ± 51.6
Mean simple RT (ms)[a]	324.7 ± 54.2	330.0 ± 59.3	317.6 ± 46.4
Regions-of-interest			
CST FA[a]	0.570 ± 0.022	0.568 ± 0.021	0.572 ± 0.022
CST MD (10^{-3} mm^2/s)[a]	0.736 ± 0.021	0.738 ± 0.020	0.734 ± 0.022
Neostriatal MD (10^{-3} mm^2/s)[b]	0.809 ± 0.018	0.810 ± 0.017	0.807 ± 0.019
Putamen MD (10^{-3} mm^2/s)[b]	0.791 ± 0.019	0.796 ± 0.018	0.786 ± 0.020
Caudate MD (10^{-3} mm^2/s)[b]	0.833 ± 0.022	0.830 ± 0.020	0.838 ± 0.024
nAcc/amygdala MD (10^{-3} mm^2/s)[b]	0.858 ± 0.022	0.852 ± 0.019	0.862 ± 0.024

Abbreviations: RT = reaction time, CST = corticospinal tract, FA = fractional anisotropy, MD = mean diffusivity, nAcc = nucleus accumbens.
[a] Data from 75 subjects.
[b] Data from 69 subjects.

Follow-up analysis, testing the anatomical specificity of the observed MD effect, showed that CST MD remained significant when including mean MD of the whole skeleton in the model (Table $3_{(2b)}$), suggesting that the association between 5-choice RT and MD in the CSTs is not mediated by a global decrease in MD. Assessing the relative contribution of the ipsi- and contralateral CST to the observed effect revealed that MD in both the ipsilateral ($\beta = 0.326$, $p = 0.005$) and contralateral CST ($\beta = 0.339$, $p = 0.004$) were significantly and positively associated with 5-choice RT, suggesting a bilateral CST effect. Moreover, the CST MD remained a significant predictor of 5-choice RT ($\beta = 0.204$, $p = 0.003$) when including simple RT ($\beta = 0.701$, $p = 10^{-14}$) as a covariate in the model. By itself, simple RT did not exhibit a significant relationship with CST MD ($\beta = 0.15$, $p = 0.18$).

Further exploration of the nature of the observed CST MD effect revealed that faster 5-choice RT was significantly associated with both lower CST $\lambda_{||}$ ($\beta = 0.222$, $p = 0.023$) and lower CST $\lambda\perp$ ($\beta = 0.244$, $p = 0.023$) when modelled individually. When entering CST $\lambda_{||}$ and CST $\lambda\perp$ as simultaneous predictors of 5-choice RT, both $\lambda_{||}$ and $\lambda\perp$ of the CST approached significance ($\lambda_{||}$: $\beta = 0.189$, $p = 0.051$; $\lambda\perp$: $\beta = 0.207$, $p = 0.051$), suggesting that the effects of CST $\lambda_{||}$ and CST $\lambda\perp$ are relatively independent.

Associations between 5-choice RT and mean diffusivity of the neostriatum

Testing our main hypothesis regarding neostriatal MD revealed that faster 5-choice RT was significantly associated with lower neostriatal MD (Table $4_{(4)}$, Fig. 4b). Further, this association became stronger when excluding age from the model (Table $4_{(4a)}$).

Follow-up analysis showed that the association between 5-choice RT and neostriatal MD remained significant (Table $4_{(4b)}$) when including nAcc/amygdala MD in the model as a control region, suggesting that the effects are relatively specific to the neostriatum. Further, MD in both the ipsilateral ($\beta = 0.319$, $p = 0.005$) and the contralateral neostriatum ($\beta = 0.379$, $p = 0.044$) were significantly and positively associated with 5-choice RT when modelled separately. Moreover, neostriatal MD ($\beta = 0.157$, $p = 0.031$) remained a significant predictor of 5-choice RT when including simple RT ($\beta = 0.720$, $p = 10^{-14}$) as an additional covariate in the model. By itself, simple RT was not significantly associated with neostriatal MD ($\beta = 0.183$, $p = 0.122$).

Post hoc analyses showed that faster 5-choice RT was associated with higher neostriatal FA ($\beta = -0.218$, $p = 0.044$), and that this association became stronger ($\beta = -0.401$, $p = 0.0008$), when excluding age from

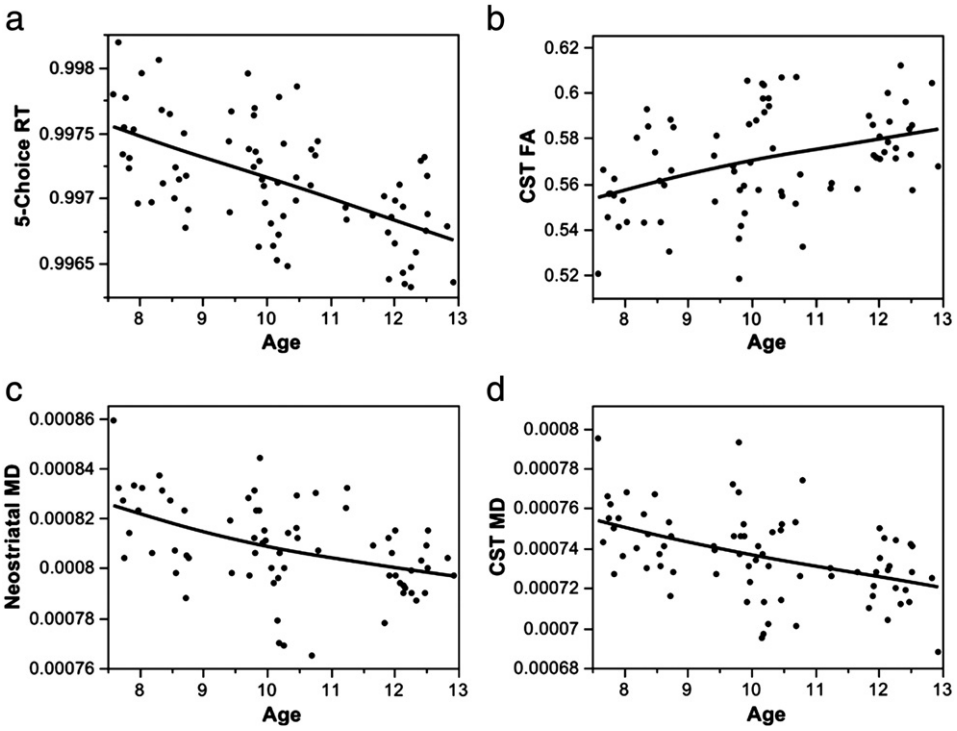

Fig. 3. Scatterplots of a) 5-choice reaction time (RT — transformed values), b) corticospinal tract (CST) FA, c) neostriatal MD and d) CST MD by age (in years). To visualise the relationships across age, a model-free smoothing spline ($\lambda = 70$) was applied to the data.

the model. However, when including nAcc/amygdala FA as an additional covariate in the model, the neostriatal FA association with 5-choice RT only approached significance ($\beta = -0.212$, $p = 0.054$). Further, the relationship between 5-choice RT and neostriatal FA did not remain significant when entering simple RT in the model (FA: $\beta = 0.088$, $p = 0.21$; simple RT: $\beta = 0.733$, $p = 10^{-13}$). By itself, simple RT was not significantly correlated with neostriatal FA ($\beta = -0.176$, $p = 0.12$).

Relative contributions of caudate nucleus and putamen in predicting 5-choice RT

Results from the follow-up analyses of regional MD in the putamen and caudate nuclei are given in Table 4. Faster 5-choice RT was significantly associated with lower MD in both the caudate (Table $4_{(4)}$) and the putamen (Table $4_{(5)}$), and the effects became stronger when excluding age as a covariate in the models (Table $4_{(4a,5a)}$). Further, effects of caudate and putamen MD remained significant when including nAcc/amygdalar MD as an additional covariate in the models (Table $4_{(4b,5b)}$).

Follow-up analyses were performed to assess the potential influence of individual variation in striatal volumes on the observed effects by including the relative volume of the putamen or caudate nucleus as an additional covariate in the models. Both caudate MD ($\beta = 0.261$, $p = 0.018$) and putamen MD ($\beta = 0.231$, $p = 0.046$) remained significant predictors of 5-choice RT when including, respectively, caudate volume ($\beta = -0.066$, $p = 0.51$) and putamen volume ($\beta = 0.012$, $p = 0.91$) in the models, suggesting that the association between neostriatal MD and 5-choice RT is not mediated by differences in striatal volumes. By themselves, neither caudate volume nor putamen volume was significantly associated with 5-choice RT ($ps \geq 0.49$). Moreover, neither caudate MD, nor putamen MD was significantly correlated with, respectively, caudate volume ($\beta = -0.030$, $p = 0.83$) or putamen volume ($\beta = 0.288$, $p = 0.095$), indicating that volume and MD may reflect distinct biological properties of the neostriatum.

Post hoc analyses revealed that higher FA in the putamen ($\beta = -0.228$, $p = 0.007$), but not in the caudate nuclei ($\beta = -0.057$, $p = 0.59$), was significantly associated with faster 5-choice RT. When subsequently examining $\lambda_{||}$ and $\lambda\perp$ diffusivities, faster 5-choice

Table 3
Multiple linear regression models predicting 5-choice reaction time with diffusion parameters within the corticospinal tracts.

		Corticospinal tracts		Gender		Age		Whole skeleton	
Model	R^2	β	p	β	p	β	p	β	p
Fractional anisotropy									
1	0.374	−0.176	0.095			−0.505	$<10^{-5}$		
Mean diffusivity									
2	0.424	0.310	**0.004**	0.010	0.910	−0.433	<0.0001		
2a	0.276	0.510	**0.000004**	0.001	0.994				
2b	0.455	0.715	**0.002**	−0.028	0.985	−0.457	<0.0001	−0.451	0.049

Each row in the table represents a separate regression model. Models 1 and 2 were adjusted for age, gender and handedness. Model 2a was adjusted for gender and handedness. Model 2b was adjusted for age, gender, handedness and whole skeleton MD. For each model, R2 is given in the leftmost column, and the regression coefficient (β) and the significance level (p) are given for each variable included in the model. Significant p-values for the primary variable of interest (corticospinal tracts) are in bold. Handedness effects were non-significant ($ps \geq 0.27$), and are not included in the table. All models included data from 75 subjects.

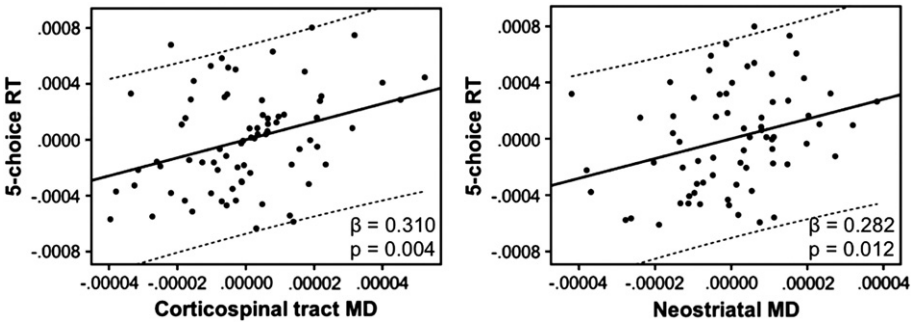

Fig. 4. Partial regression plots of the 5-choice reaction time (RT) as a function of MD within the (a) corticospinal tracts or (b) neostriatum, adjusted for age, gender and handedness. The regression coefficient (β) and the significance level (p) for each MD variable are given in the lower right corner of each plot. Note that residuals are plotted.

RT was significantly associated with both $\lambda\perp$ ($\beta = 0.278$, $p = 0.014$) and $\lambda_{||}$ ($\beta = 0.230$, $p = 0.038$) of the caudate nucleus, but only with $\lambda\perp$ ($\beta = 0.265$, $p = 0.019$) and not $\lambda_{||}$ ($\beta = 0.174$, $p = 0.12$) of the putamen. Putamen FA remained a significant predictor of 5-choice RT ($\beta s \leq -0.288$, $ps \leq 0.010$) when including either nAcc/amygdala FA ($\beta = 0.004$, $p = 0.97$) or putamen volume ($\beta = 0.002$, $p = 0.98$) as additional covariates in the model.

Follow-up analyses assessed the relative contributions of MD in the ipsi- and contralateral putamen and caudate on 5-choice RT. When modelled individually, the effects of ipsilateral ($\beta = 0.221$, $p = 0.050$) and contralateral ($\beta = 0.215$, $p = 0.051$) putamen MD on 5-choice RT were of similar size, suggesting that the effect of putamen MD was bilateral. However, for caudate MD, the association between 5-choice RT and MD in the ipsilateral caudate ($\beta = 0.310$, $p = 0.008$) was somewhat stronger than that for the contralateral caudate ($\beta = 0.180$, $p = 0.097$), which only approached significance. To further investigate the laterality of the caudate MD effect, post hoc analyses were conducted, in which ipsi- and contralateral caudate MD were included in the same model. When modelled simultaneously, ipsilateral ($\beta = 0.312$, $p = 0.038$), but not contralateral caudate MD ($\beta = -0.003$, $p = 0.98$) exhibited a significant relationship with 5-choice RT. Analysing the right-handers ($n = 63$) and left-handers ($n = 6$) separately revealed that for the right-handers, MD in the right caudate ($\beta = 0.309$, $p = 0.050$), but not the left caudate ($\beta = -0.013$, $p = 0.93$) exhibited a relationship with 5-choice RT. For the left-handed subjects, 5-choice RT appeared to exhibit a stronger, though not significant, relationship with MD in the right caudate ($\beta = 1.244$, $p = 0.23$) relative to that of the left caudate ($\beta = -0.048$, $p = 0.92$). Thus, the association between 5-choice RT and caudate MD may be, to some degree, lateralized.

Effect-size maps

The primary goal of this study was to test specific anatomical hypotheses about the relationship between microstructure of the CST and neostriatum and variability in 5-choice RT performance in children. Therefore neither a whole brain, voxel-wise analysis of the effects (appropriately adjusted for test-multiplicity), nor a restricted voxel-wise analysis with small volume correction was deemed appropriate for testing these a priori hypotheses. However, since the analyses we used produce estimates of the effect size at each voxel, we have provided visualisation of the effect-size maps. The maps show the distribution of t-values in skeleton (Fig. 5) or neostriatal (Fig. 6) voxels and thus, provide complementary information about the regional distribution of associations between 5-choice RT performance and MD in the brain, adjusted for age and gender.

For the right-handed children only, the map of the TBSS skeleton revealed some areas with apparent relationships between MD and 5-choice RT performance comparable with those in the CSTs (Fig. 4), although it should be emphasised that these maps show uncorrected t-values. The symmetric skeleton as a whole contained 102,154 voxels, of which 10,308 voxels, or 10.1%, displayed t-values greater than 1.995 (a value associated with an uncorrected $p<0.05$). In comparison, 38.0% of the voxels within the left CST ROI and 34.0% of the voxels within the right CST ROI had t-values exceeding this value. Additionally, to further compare the results from the ROI analyses with the number of uncorrected significant voxels within the CSTs, a t-map based on all 75 subjects (left-handers left–right flipped) included in the CST ROI analyses was generated (not shown). In this map, 9.6% of the skeleton voxels had associated t-values greater than 1.995, whilst 43.3% of the voxels within the ipsilateral CST ROI and

Table 4
Multiple linear regression models predicting 5-choice RT with mean diffusivity (MD) of striatal regions-of-interest (ROIs).

		MD in ROI*		Gender		Age		nAcc/amygdala MD	
Model	R^2	β	p	β	p	β	p	β	p
**Neostriatum*									
3	0.400	0.282	**0.012**	0.018	0.854	−0.451	0.0001		
3a	0.238	0.485	**0.00003**	−0.002	0.988				
3b	0.402	0.311	**0.019**	0.029	0.779	−0.450	0.0001	−0.052	0.672
**Caudate nuclei*									
4	0.395	0.271	**0.017**	0.088	0.385	−0.458	<0.0001		
4a	0.227	0.478	**0.00005**	0.031	0.779				
4b	0.397	0.260	**0.027**	0.075	0.482	−0.452	0.0001	−0.044	0.682
**Putamen*									
5	0.381	0.234	**0.037**	−0.016	0.881	−0.489	<0.0001		
5a	0.178	0.429	**0.0005**	−0.067	0.572				
5b	0.384	0.284	**0.057**	−0.010	0.927	−0.487	<0.0001	−0.073	0.600

* MD of ROIs in either the Neostriatum, Caudate Nuclei or the Putamen. Each row in the table represents a separate regression model. Models 3, 4 and 5 were adjusted for age, gender and handedness. Models with 'a' were adjusted for gender and handedness. Models with 'b' were adjusted for age, gender, handedness, and nucleus accumbens (nAcc)/amygdala MD. For each model, R^2 is given in the leftmost column, and the regression coefficient (β) and the significance level (p) are given for each variable included in the model. Significant p-values for the primary variable of interest (MD in ROI) are in bold. Handedness effects were non-significant ($ps \geq 0.29$), and are not included in the table. All models included data from 69 subjects.

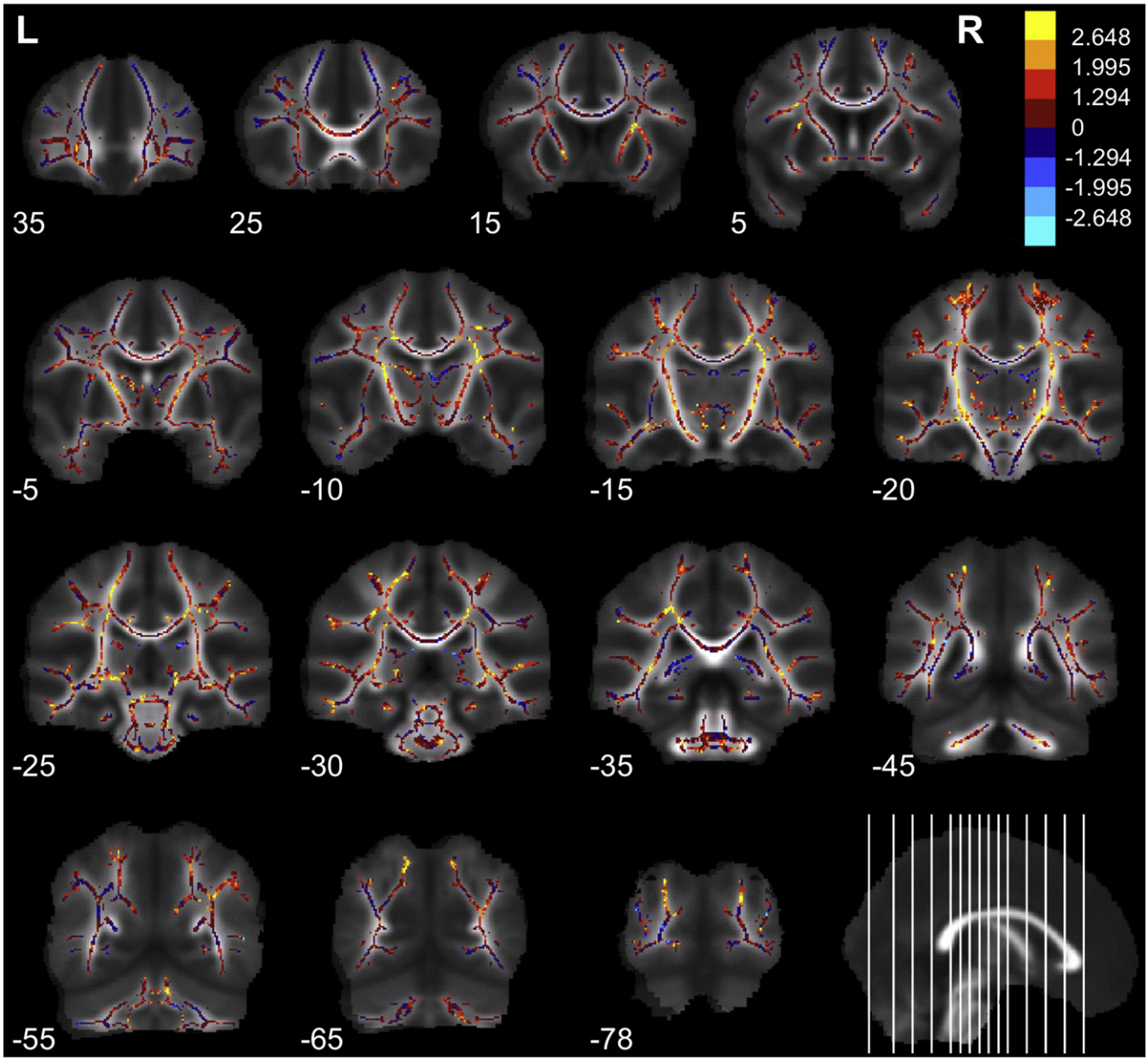

Fig. 5. Effect-size map based on data from the right-handed subjects (N = 66) of the association between 5-choice reaction time and mean diffusivity, adjusted for age and gender. The effect-size map is overlaid on the mean symmetric FA images. The association of faster 5-choice RT with lower MD values yields positive t-values shown in warm colours, whilst negative t-values are shown in cool colours. The colour bar shows the colour mapping of all skeleton voxels to the values of the uncorrected t-statistics (t = 0 = p = 1; t = ±1.294 = p = 0.2; t = ± 1.995 = p = 0.05; t = ± 2.648 = p = 0.01). The MNI coordinates for the coronal images are given under each image. In the lower right corner, the coronal slices shown are depicted on the midsagittal image with the coronal slice 35 displayed to the far left and coronal image −78 to the far right. Images are shown with the subject's right side on the right (neurological convention). The CST ROIs were located between slice −10 and −35.

62.0% of the voxels within the contralateral CST ROI had t-values exceeding this value.

From the map of the skeleton voxels (Fig. 5), several clusters exceeding t-values greater than 1.995 were apparent. Amongst these were clusters located in the right inferior fronto-occipital fasciculus/uncinate fasciculus (cluster not shown), bilateral cingulum (slices −15 to −25), left superior longitudinal fasciculus (slice −25), and in the white matter underlying the precuneus (slice −65) and cuneus (slice −78) cortices bilaterally, in addition to a number of smaller clusters visible in the effect-size map. Interestingly, the effect-size map of the neostriatum revealed that some regions of the neostriatum appear to exhibit a closer relationship with 5-choice RT than others (Fig. 6). An apparent ventrorostral to dorsocaudal gradient of low to high t-values was observed in the putamen, most notable in the two sagittal images.

Discussion

The present study examined associations between 5-choice RT performance and microstructure within the motor network in children aged 7 to 13 years. As hypothesised, faster choice RT was significantly associated with lower CST and neostriatal MD, adjusted for age, gender and handedness. Effects of CST and putamen MD were bilateral, whilst MD in right caudate nucleus exhibited a stronger relationship with 5-choice RT than did MD in the left caudate nucleus. Because both RTs (Kail, 1991) and MD (Lebel et al., 2008) decrease throughout childhood and adolescence, a simple correlation between these measures could represent a non-specific association attributable to unmeasured factors that are indexed by chronological age (for further discussion see Madsen et al., 2010). Thus, we hypothesised

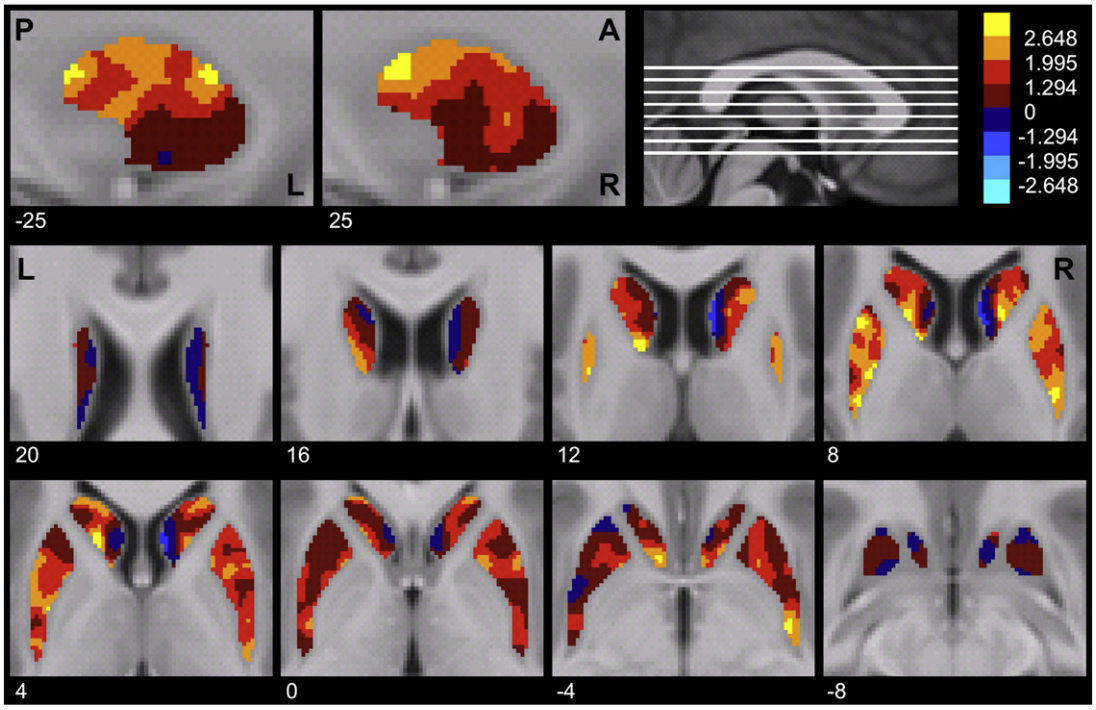

Fig. 6. Effect-size map based on the right-handed subjects (N = 63) of the association between 5-choice reaction time and mean diffusivity (MD), adjusted for age and gender. The effect-size map is overlaid on the symmetric average of the DARTEL-warped T_1-images of all subjects. The association of faster 5-choice RT with lower MD values yields positive t-values shown in warm colours, whilst negative t-values are shown in cool colours. The colour bar shows the colour mapping of voxels within caudate nucleus, putamen and nucleus accumbens to the values of the uncorrected t-statistics ($t = 0 = p = 1$; $t = \pm 1.294 = p = 0.2$; $t = \pm 1.995 = p = 0.05$; $t = \pm 2.648 = p = 0.01$). Two sagittal slices through the left and right putamen are shown in the top row, and 8 axial slices are shown in the lower 2 rows. Coordinates in 'DARTEL space' are given under each image. Top right, the axial slices shown are depicted on the midsagittal image with the axial slice 20 representing the most superior slice shown and axial slice −8 the most inferior. Axial images are shown with the subject's right side on the right (neurological convention).

that the association between 5-choice RT and motor system MD would remain significant after controlling for age, i.e., that even amongst children of similar age, those with lower CST and neostriatal MD would exhibit faster choice RT. These hypotheses were confirmed.

Our follow-up analyses provided further clues about the nature of these associations. First, we addressed the question whether the associations between 5-choice RT and microstructure within the CSTs and neostriatum were anatomically specific, i.e., the extent to which 5-choice RT exhibited a relatively specific relationship to MD in these regions relative to others. This is an important question, since MD decreases concurrently in many brain regions during childhood and adolescence (Eluvathingal et al., 2007; Lebel et al., 2008). The relationship between 5-choice RT of CST and neostriatal MD remained significant when including, respectively, whole skeleton MD or nAcc/amygdalar MD as covariates in the models. Therefore, we infer that the relationship between 5-choice RT and MD within these regions is not likely to be driven by global MD differences, but may be more strongly related to the microstructure of specific regions.

Analyses of $\lambda_{||}$ and $\lambda\perp$ showed that faster 5-choice RT was associated with both lower $\lambda_{||}$ and lower $\lambda\perp$ in the CSTs. These findings may explain why we only observed effects of CST MD, and not of CST FA. Although interpretation of differences in DTI parameters is not straightforward, some studies suggest that $\lambda\perp$ may be more sensitive to changes in myelination, extracellular volume fraction, and axonal density (Schwartz et al., 2005; Song et al., 2003, 2005), whilst $\lambda_{||}$ may be more sensitive to differences in axonal diameter (Schwartz et al., 2005). Using a mouse model of retinal ischemia, a DTI and histology study revealed a gradual decrease in relative anisotropy, caused by, at first, decrease in $\lambda_{||}$, corresponding with the timing of axonal degeneration, followed by increase in $\lambda\perp$, associated with optic nerve demyelination (Song et al., 2003). Moreover, a study of the normal rat cervical spinal cord found that the perpendicular apparent diffusion coefficient (ADC), a measure similar to MD, was positively correlated with extracellular volume fraction and axonal spacing, and negatively correlated with axonal number and myelination. Further, parallel ADC was found to be positively correlated with axonal diameter, and negatively with axonal number (Schwartz et al., 2005). It should be noted that other tissue parameters, such as axon density and tortuosity, crossing fibres and tract geometry may also contribute to differences in $\lambda\perp$ and $\lambda_{||}$ (Beaulieu, 2009; Schwartz et al., 2005). Whatever the neuroanatomical correlate of $\lambda\perp$ or $\lambda_{||}$ might be, our observation of similar effects of $\lambda\perp$ and $\lambda_{||}$ provides no further evidence regarding the cellular basis of these effects.

We also sought evidence that variability in the volumes of putamen and caudate might be relevant to our effects, and we found none. The relationship between choice RT and neostriatal MD remained significant when including the relative volumes as additional covariates in the models, suggesting that the effects are more closely linked to the microstructure than to the volumes of these structures. The neurobiological underpinnings that account for individual variations of MD and other diffusion measures in grey matter structures are poorly understood, particularly in healthy individuals. Water diffusion is hindered by cellular structures, particularly cell membranes, and thus individual variations in diffusion parameters in grey matter could be due to variations in membrane density, tortuosity and/or permeability. Lower MD has been related to higher cell density in tumours (Chenevert et al., 2006; Gibbs et al., 2009). Moreover, a recent study in rats found that over an 18-month period after radiation treatment temporal changes in ADC were negatively correlated with changes in glial cell staining in the hippocampus (Huang et al., 2010). Although MD does not measure cell density directly, these findings suggest that differences in neuronal and glial cell densities may contribute to the observed neostriatal effects in the present study. Notably, with few regional exceptions (e.g. hippocampus) neuron density is generally considered to be stable within the age range studied (7 to 13 years). Whether

glial proliferation occurs in the later childhood and early adolescent years is unknown. Furthermore, many other tissue parameters may influence the regional magnitude of water diffusion, including cell number and size, membrane permeability (Chenevert et al., 2006), or number, size and tortuosity of neostriatal axons, dendrites and astrocytic processes.

We also examined the mediating role of simple RT on the observed effects. The MD effects on 5-choice RT remained significant when including simple RT in the models, suggesting that the increased task demand for response selection may be particularly relevant to the association between choice RT and motor system MD in normal children. Alternatively, this pattern may be related to more general differences in task difficulty.

TBSS improves inter-subject registration of brain fibre tracts relative to prior methods for performing spatial normalisation of FA images (Smith et al., 2006) and the method obviates the need for extensive spatial smoothing. After applying TBSS to align the tracts across subjects we averaged FA over the segments of the tract skeleton that corresponded to the expected location of the corticospinal tracts. This was considered to be a more objective way of estimating diffusion measures within a comparable portion of the tract within each individual than subjective (manual) delineation of regions within the white matter, and a more powerful test of our hypothesis than a voxel-wise approach. However, the method produces only an approximation of the diffusion measures in the targeted tracts. Future studies employing well validated tractography methods defining tracts based on connectivity, or methods using probabilistic atlases (Hagler et al., 2009) may provide more definitive assessments of microstructure in particular fibre tracts in vivo.

Previous studies of young adults examining relationships between choice RT and white matter microstructure generally employed more complex choice RT tasks that also placed high demands on visual discrimination, response inhibition, and/or working memory (Konrad et al., 2009; Madden et al., 2004; Tuch et al., 2005). These studies mainly focused on regions outside the motor system and found effects in pathways supporting visuospatial attention. The choice RT task used in the present study requires response selection and initiation, but places little demand on visual discrimination, response inhibition, or working memory. Thus, we focused on relationships with regions within the motor system known to be involved in movement selection and execution (Gerardin et al., 2004). However, in the TBSS effect-size map (Fig. 5), some clusters exhibiting an apparent relationship with choice RT are present in regions similar to those found in adults (Konrad et al., 2009; Tuch et al., 2005), suggesting that regions supporting visuospatial attention may also be related to children's performance on the present task. Future studies are necessary to address this in more detail.

In the effect-size map of the neostriatum (Fig. 6), an apparent ventrorostral to dorsocaudal gradient of low to high t-values may be observed in the putamen. Previous studies have shown a rostrocaudal functional gradient of inputs in the neostriatum, where motor and premotor cortices mainly project to dorsal and caudal areas of the putamen (Draganski et al., 2008; Haber, 2003; Haber and Gdowski, 2004; Lehericy et al., 2004), suggesting that the putamen voxels with high t-values observed in the present study may be within the regions involved in motor control. However, further studies are needed to elucidate the relationship between choice RT performance and MD within specific neostriatal regions.

Our findings suggest that even amongst children of similar age, lower MD within core motor structures is associated with faster 5-choice RTs. Questions remain regarding the neurobiological interpretation of such age-adjusted relationships between individual variability in MD and choice RT. This structure–function relationship may reflect individual differences in the maturational trajectories of the motor system, i.e., differences in the phase of CST and neostriatal maturation amongst children of similar age. It is plausible that this variability could mediate, at least to some extent, the associations found in the present study, since both microstructure (Lebel et al., 2008) and RTs (Kail, 1991) continue to develop across this age range. Alternatively, the variability in motor system MD may reflect individual differences in the architecture of the motor system (perhaps differences in the underlying connectivity) that emerge earlier during brain development and remain stable in spite of superimposed biological changes associated with maturation. This is plausible since individual differences in behavioural performance have been associated with MD variability in adults (Konrad et al., 2009; Piras et al., 2010) as well as children.

It is also possible that dynamic processes, perhaps associated with activity levels in the neural circuits throughout childhood, could influence the microstructure within the motor network. A recent study of adults examined changes in DTI parameters in connection with 6 weeks of practice in a complex whole-body balancing task, observing negative correlations between improvements in motor performance and MD changes in bilateral anterior centrum semiovale, left brain stem, and right internal capsule. These findings were interpreted as learning-related increases in cell density or axonal/dendritic arborization hindering the diffusion of water molecules (Taubert et al., 2010). Thus, the individual differences observed in the present study could reflect variability in sensorimotor experiences and skill acquisition of the children, which may have influenced the grey and white matter microstructure, e.g., cell density, axonal or dendritic arborization and/or myelination.

Conclusions

Individual differences in 5-choice RT performance were associated with individual differences in MD within the CSTs and neostriatum. These relationships were not attributable to age and did not appear to reflect behavioural effects of a more general maturational decrease in MD across the brain. Children of similar age may vary in the phase of maturation in the motor network, and this variability may mediate the observed associations. The associations could also be mediated by more stable individual differences in the architecture of the motor system, or to more transient differences associated with dynamic (perhaps activity-dependent) processes. Longitudinal observations are needed to further clarify these important questions.

Acknowledgments

This work was supported by the Danish Medical Research Council and the Lundbeck Foundation.

References

Andersson, J.L., Hutton, C., Ashburner, J., Turner, R., Friston, K., 2001. Modeling geometric deformations in EPI time series. Neuroimage 13, 903–919.
Andersson, J.L.R., Jenkinson, M., Smith, S., 2007. Non-linear optimisation and non-linear registration, aka spatial normalisation. FMRIB technical report TR07JA1 and TR07JA2. www.fmrib.ox.ac.uk/analysis/techrep.
Ashburner, J., 2007. A fast diffeomorphic image registration algorithm. Neuroimage 38, 95–113.
Ashburner, J., Friston, K.J., 2005. Unified segmentation. Neuroimage 26, 839–851.
Basser, P.J., Mattiello, J., LeBihan, D., 1994. MR diffusion tensor spectroscopy and imaging. Biophys. J. 66, 259–267.
Beaulieu, C., 2009. Gaussian modeling of the diffusion signal. In: Johansen-Berg, H., Behrens, T.E.J. (Eds.), Diffusion MRI: From Quantitative Measurement to In-Vivo Neuroanatomy. Elsevier, London, UK, pp. 105–126.
Bohr, S., Gullmar, D., Knab, R., Reichenbach, J.R., Witte, O.W., Haueisen, J., 2007. Fractional anisotropy correlates with auditory simple reaction time performance. Brain Res. 1186, 194–202.
Chang, L.C., Jones, D.K., Pierpaoli, C., 2005. RESTORE: robust estimation of tensors by outlier rejection. Magn. Reson. Med. 53, 1088–1095.
Chenevert, T.L., Sundgren, P.C., Ross, B.D., 2006. Diffusion imaging: insight to cell status and cytoarchitecture. Neuroimaging Clin. N. Am. 16, 619–632 (viii-ix).
Cuadra, M.B., Cammoun, L., Butz, T., Cuisenaire, O., Thiran, J.P., 2005. Comparison and validation of tissue modelization and statistical classification methods in T1-weighted MR brain images. IEEE Trans. Med. Imaging 24, 1548–1565.

Draganski, B., Kherif, F., Kloppel, S., Cook, P.A., Alexander, D.C., Parker, G.J., Deichmann, R., Ashburner, J., Frackowiak, R.S., 2008. Evidence for segregated and integrative connectivity patterns in the human basal ganglia. J. Neurosci. 28, 7143–7152.

Eluvathingal, T.J., Hasan, K.M., Kramer, L., Fletcher, J.M., Ewing-Cobbs, L., 2007. Quantitative diffusion tensor tractography of association and projection fibers in normally developing children and adolescents. Cereb. Cortex 17, 2760–2768.

Gerardin, E., Pochon, J.B., Poline, J.B., Tremblay, L., Van de Moortele, P.F., Levy, R., Dubois, B., Le Bihan, D., Lehericy, S., 2004. Distinct striatal regions support movement selection, preparation and execution. Neuroreport 15, 2327–2331.

Gibbs, P., Liney, G.P., Pickles, M.D., Zelhof, B., Rodrigues, G., Turnbull, L.W., 2009. Correlation of ADC and T2 measurements with cell density in prostate cancer at 3.0 Tesla. Invest. Radiol. 44, 572–576.

Haber, S.N., 2003. The primate basal ganglia: parallel and integrative networks. J. Chem. Neuroanat. 26, 317–330.

Haber, S.N., Gdowski, M.J., 2004. The basal ganglia. In: Paxinos, G., Mai, J.K. (Eds.), The Human Nervous System. Elsevier, London.

Hagler Jr., D.J., Ahmadi, M.E., Kuperman, J., Holland, D., McDonald, C.R., Halgren, E., Dale, A.M., 2009. Automated white-matter tractography using a probabilistic diffusion tensor atlas: application to temporal lobe epilepsy. Hum. Brain Mapp. 30, 1535–1547.

Hua, K., Zhang, J., Wakana, S., Jiang, H., Li, X., Reich, D.S., Calabresi, P.A., Pekar, J.J., van Zijl, P.C., Mori, S., 2008. Tract probability maps in stereotaxic spaces: analyses of white matter anatomy and tract-specific quantification. Neuroimage 39, 336–347.

Huang, L., Smith, A., Badaut, J., Obenaus, A., 2010. Dynamic characteristics of 56Fe-particle radiation-induced alterations in the rat brain: magnetic resonance imaging and histological assessments. Radiat. Res. 173, 729–737.

Jernigan, T.L., Trauner, D.A., Hesselink, J.R., Tallal, P.A., 1991. Maturation of human cerebrum observed in vivo during adolescence. Brain 114 (Pt 5), 2037–2049.

Jernigan, T.L., Gamst, A.C., Fennema-Notestine, C., Ostergaard, A.L., 2003. More "mapping" in brain mapping: statistical comparison of effects. Hum. Brain Mapp. 19, 90–95.

Jovicich, J., Czanner, S., Greve, D., Haley, E., van der Kouwe, A., Gollub, R., Kennedy, D., Schmitt, F., Brown, G., Macfall, J., Fischl, B., Dale, A., 2006. Reliability in multi-site structural MRI studies: effects of gradient non-linearity correction on phantom and human data. Neuroimage 30, 436–443.

Kail, R., 1991. Developmental change in speed of processing during childhood and adolescence. Psychol. Bull. 109, 490–501.

Konrad, A., Vucurevic, G., Musso, F., Stoeter, P., Winterer, G., 2009. Correlation of brain white matter diffusion anisotropy and mean diffusivity with reaction time in an oddball task. Neuropsychobiology 60, 55–66.

Lebel, C., Walker, L., Leemans, A., Phillips, L., Beaulieu, C., 2008. Microstructural maturation of the human brain from childhood to adulthood. Neuroimage 40, 1044–1055.

Lehericy, S., Ducros, M., Krainik, A., Francois, C., Van de Moortele, P.F., Ugurbil, K., Kim, D.S., 2004. 3-D diffusion tensor axonal tracking shows distinct SMA and pre-SMA projections to the human striatum. Cereb. Cortex 14, 1302–1309.

Madden, D.J., Whiting, W.L., Huettel, S.A., White, L.E., MacFall, J.R., Provenzale, J.M., 2004. Diffusion tensor imaging of adult age differences in cerebral white matter: relation to response time. Neuroimage 21, 1174–1181.

Madsen, K.S., Baare, W.F., Vestergaard, M., Skimminge, A., Ejersbo, L.R., Ramsoy, T.Z., Gerlach, C., Akeson, P., Paulson, O.B., Jernigan, T.L., 2010. Response inhibition is associated with white matter microstructure in children. Neuropsychologia 48, 854–862.

Miller, J.O., Low, K., 2001. Motor processes in simple, go/no-go, and choice reaction time tasks: a psychophysiological analysis. J. Exp. Psychol. Hum. Percept. Perform. 27, 266–289.

Niogi, S.N., McCandliss, B.D., 2006. Left lateralized white matter microstructure accounts for individual differences in reading ability and disability. Neuropsychologia 44, 2178–2188.

Piras, F., Caltagirone, C., Spalletta, G., 2010. Working memory performance and thalamus microstructure in healthy subjects. Neuroscience 171, 496–505.

Reese, T.G., Heid, O., Weisskoff, R.M., Wedeen, V.J., 2003. Reduction of eddy-current-induced distortion in diffusion MRI using a twice-refocused spin echo. Magn. Reson. Med. 49, 177–182.

Schwartz, E.D., Cooper, E.T., Fan, Y., Jawad, A.F., Chin, C.L., Nissanov, J., Hackney, D.B., 2005. MRI diffusion coefficients in spinal cord correlate with axon morphometry. Neuroreport 16, 73–76.

Smith, S.M., Jenkinson, M., Woolrich, M.W., Beckmann, C.F., Behrens, T.E., Johansen-Berg, H., Bannister, P.R., De Luca, M., Drobnjak, I., Flitney, D.E., Niazy, R.K., Saunders, J., Vickers, J., Zhang, Y., De Stefano, N., Brady, J.M., Matthews, P.M., 2004. Advances in functional and structural MR image analysis and implementation as FSL. Neuroimage 23 (Suppl. 1), S208–S219.

Smith, S.M., Jenkinson, M., Johansen-Berg, H., Rueckert, D., Nichols, T.E., Mackay, C.E., Watkins, K.E., Ciccarelli, O., Cader, M.Z., Matthews, P.M., Behrens, T.E., 2006. Tract-based spatial statistics: voxelwise analysis of multi-subject diffusion data. Neuroimage 31, 1487–1505.

Snook, L., Paulson, L.A., Roy, D., Phillips, L., Beaulieu, C., 2005. Diffusion tensor imaging of neurodevelopment in children and young adults. Neuroimage 26, 1164–1173.

Song, S.K., Sun, S.W., Ju, W.K., Lin, S.J., Cross, A.H., Neufeld, A.H., 2003. Diffusion tensor imaging detects and differentiates axon and myelin degeneration in mouse optic nerve after retinal ischemia. Neuroimage 20, 1714–1722.

Song, S.K., Yoshino, J., Le, T.Q., Lin, S.J., Sun, S.W., Cross, A.H., Armstrong, R.C., 2005. Demyelination increases radial diffusivity in corpus callosum of mouse brain. Neuroimage 26, 132–140.

Sowell, E.R., Thompson, P.M., Holmes, C.J., Jernigan, T.L., Toga, A.W., 1999. In vivo evidence for post-adolescent brain maturation in frontal and striatal regions. Nat. Neurosci. 2, 859–861.

Taubert, M., Draganski, B., Anwander, A., Muller, K., Horstmann, A., Villringer, A., Ragert, P., 2010. Dynamic properties of human brain structure: learning-related changes in cortical areas and associated fiber connections. J. Neurosci. 30, 11670–11677.

Tuch, D.S., Salat, D.H., Wisco, J.J., Zaleta, A.K., Hevelone, N.D., Rosas, H.D., 2005. Choice reaction time performance correlates with diffusion anisotropy in white matter pathways supporting visuospatial attention. Proc. Natl. Acad. Sci. U. S. A. 102, 12212–12217.

Vestergaard, M., Madsen, K.S., Baare, W.F., Skimminge, A., Ejersbo, L.R., Ramsoy, T.Z., Gerlach, C., Akeson, P., Paulson, O.B., Jernigan, T.L., 2011. White matter microstructure in superior longitudinal fasciculus associated with spatial working memory performance in children. J. Cogn. Neurosci. 23, 2135–2146.